INFLUENCE OF TARGET STRENGTH ON LOW-VELOCITY CRATERING: 3-D SIMULATIONS

W. A. Watters[1] (**wwatters@wellesley.edu**), T. M. Davison,[2] and G. S. Collins;[2] [1]Dept. Astronomy, Whitin Observatory, Wellesley College; [2]Impact & Astromaterials Research Centre, Dept. Earth Science & Eng., Imperial College London.

Low-velocity impacts in strong materials have received relatively little attention from modeling studies since the introduction of realistic strength and damage models in impact hydrocodes [e.g., 1,2,3]. We present the results of 3-D simulations of low-velocity impacts to examine the dependence of crater shape on target strength and impact velocity in the range 0.5 km/s $\leq v_i \leq$ 2.0 km/s. Our goals are to identify and understand the origin of structural and morphometric relationships characteristic of strength-dominated craters with $D \sim$ 100 m. This includes, for example, an investigation of how the distribution of strength heterogeneities influences crater growth and final planform shape [4-8]. This work has applications to understanding the small-crater population on Mars, as well as leveraging the morphometry of small craters to investigate the properties of planetary surface materials.

Model description. The impact hydrocode iSALE-3D was used to model impacts with velocities of 0.5, 1.0, 1.5, and 2.0 km/s in a symmetric half space [9,10,11]. The impact angles were 30°, 45°, and 90° with respect to horizontal. The projectile was spanned by 10 or 16 cells, with a cell size of 1 m or 0.625 m, respectively (10 m projectile radius). We used a basalt-like material model with high cohesive strength representing intact rock ("strong" target) and relatively low strength representing intergranular cohesion in regolith ("weak" target). Target and projectile materials are characterized using a model of yield strength as a function of pressure, temperature, and damage [12], and a damage model that describes scalar damage as a function of plastic strain [13]. The target is nonporous in all cases. Thermodynamic response is described by an ANEOS-derived equation of state table for basalt [14]. The model material and impact parameters are appropriate for understanding secondary impacts on Mars in strong (e.g., lava plains) and weak materials (e.g., regolith or sediments).

Results: oblique impacts. Momentum-dominated, low-speed secondary impacts are known to produce all of the following features: (a) taller rims downrange, (b) preponderance of ejecta downrange, (c) steeper cavity wall uprange, and (d) cavity planforms elongated along-range [15,16]. Impact angle may vary widely, but is likely not shallower than ~30° (see [3] for a review). We find that while features (b-d) are clearly expressed in our simulations for both strong and weak targets, the expected asymmetry of crater rim heights is not expressed in the strong target case (Fig. 1). Strength-dominated craters differ from their weak-target counterparts in all of the following ways: (i) smaller diameters, (ii) smaller depth/diameter; (iii) taller rims in the *uprange* direction; (iv) rims are shorter (1/3-1/4 the height of weak-target crater rims) but (v) exhibit greater relief; (vi) planforms exhibit marked deviations from a smooth, elliptical shape. The small-scale deviations from symmetry are hypothesized to result from strength variations created by shock damage during contact and compression.

Results: vertical impacts. To remove the along-range elongation, we also examined the case of vertical impacts for v_i = 1 km/s in weak and strong targets. As expected, the weak-target impact produces a uniform rim and smooth, continuous, circular planform, whereas the strength-dominated crater has a discontinuous and irregular rim with significant relief. We find a correlation between planform radius (of rim or cavity) and rim height as well as uplift (the latter quantity is measured as the overall vertical displacement in upper crater walls). The positive correlation between rim height and rim radius was not observed in a recent study of small, well-preserved primary craters [17], but should be observed in populations of well-preserved secondary craters in young lava plains.

For v_i = 1 km/s, we find that the size of the final cavity is comparable to the region damaged by the impact shockwave. To understand in more detail how final planform shape irregularities are influenced by strength irregularities, we compared the azimuthal dependence of average strength to the azimuthal dependence of final crater radius. In particular, we computed the correlation between the average strength in wedges measuring 20° wide and the radius of the final crater cavity along the centerline of each wedge. (Each wedge is one computational cell deep (1 m) and extends to 1.1R for average radius R). The Pearson correlation coefficient (ρ_s) for the comparison of these quantities is shown in Fig. 2A as a function of time.

The correlation between strength and final cavity radius fluctuates dramatically in the first half second, and then becomes strongly negative at ~0.7 s. That is, the final cavity planform is strongly negatively correlated with the strength field when the crater has grown to about 75% of its final size. In other words, strength variations do not strongly influence crater shape until the last 25% of crater growth for this case. Fig. 2B shows the standard deviation of cavity planform radius normalized by average radius (σ_R/R) over time for the weak and strong targets. In the latter, the deviation from radial symmetry begins to climb at roughly the

same time as ρ_s reaches its minimum value.

References: [1] Collins et al. (2011) *EPSL*, 310, pp. 1-8. [2] Davison et al. (2011) *MAPS*, 46, pp. 1510-1524. [3] Watters, W.A. et al. (2017) *JGR* (in press); [4] Shoemaker, E.M. (1960) *Int'l Geo. Cong.* 21; [5] Fulmer, C.V. & W.A. Roberts (1963) *Icarus*, 2, pp. 452-465; [6] Eppler, D.T. *GSA Bull.*, (1983) 94, pp. 274–291; [7] Öhman et al. (2008) *MAPS* 43, 10, 1605-1628; [8] Watters, W.A. et al. (2017) *Icarus*, 286, pp.15-34; [9] Amsden et al. (1980) *Los Alamos Nat'l Lab.* LA-8095; [10] Elbehausen, D. et al. (2009) *Icarus*, 204, pp. 716-731; [11] Collins, G.S. et al. (2016) iSALE Dellen User's Manual; [12] Collins, G.S. et al., (2004) *MAPS*, 39, pp. 217-231; [13] Ivanov et al., (2010) *GSA spec. pap*. 465, pp. 29-49; [14] Pierazzo et al., (2005) *GSA spec. pap.*, 384, pp. 443-457; [15] Roberts, W. (1964) *Icarus* 3, pp. 348-364; [16] Moore, H.G. (1969) *USGS prof. paper* 658-B, pp. B107-B112; [17] Watters et al. (2015) *JGR*, 120, pp. 226-254.

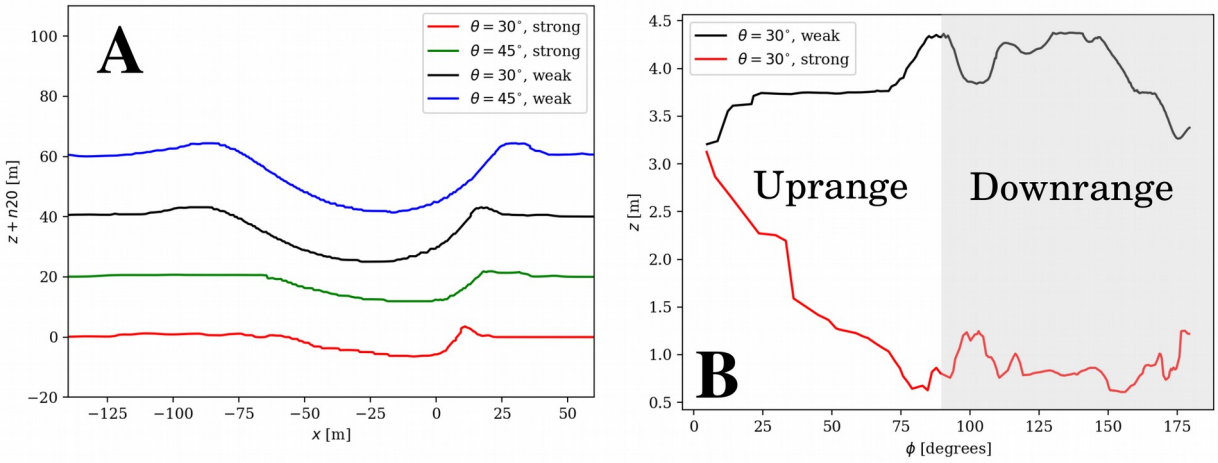

Figure 1: (A) Cross-section elevation profiles of impact craters produced in iSALE-3D simulations of low-velocity impacts (v_i = 0.5 km/s) for two impact angles (30° and 45°) in targets with high and low cohesive strength ("strong" vs. "weak"). (B) Rim elevation as a function of heading with respect to the uprange direction for the second and fourth craters shown in (A). The rim formed in strong material is lower and discontinuous (elevation drops to near zero in places), has greater overall relief, and is taller in the uprange direction.

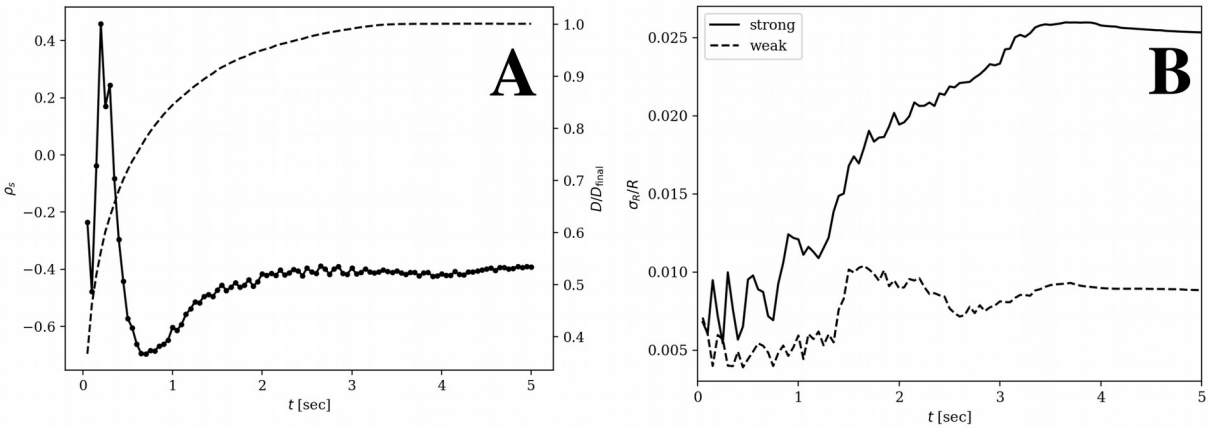

Figure 2: Plots illustrating the evolution of cavity planform asymmetry in *vertical*, low-velocity impacts (v_i = 1 km/s). (A) Pearson correlation coefficient for the comparison between *final* cavity radius (in all directions) and the *time-dependent* average strength in solid wedges (in same directions). Current diameter as a fraction of final diameter is also plotted (dashed line). The target and projectile each have high cohesive strength in this simulation (intact basalt). (B) Standard deviation of time-dependent cavity radius (σ_R), normalized by average radius (R) for strong and weak targets, defined as before.